ISSN 2079-1704. Хімія, фізика та технологія поверхні. 2024. Т. 15. № 3. С. 313-327

PACS: 31.15.Ct; 68.08.−p; 68.35.bm doi: 10.15407/hftp15.03.313

**V.M. Gun'ko, V.V. Turov**

# INTERFACIAL AND TEMPERATURE BEHAVIORS OF WATER AND SOLUTIONS BOUND TO WATER-SOLUBLE LIGNIN POWDER

*Chuiko Institute of Surface Chemistry of National Academy of Sciences of Ukraine*
*17 General Naumov Str., Kyiv, 03164, Ukraine, E-mail: vlad_gunko@ukr.net*

*Production of valuable industrial materials from lignins as byproducts of different origin is of importance to solve the utilization problem for large amounts of these byproducts. One of the corresponding pathways is the production of water-soluble lignins, for which, interactions with water and aqueous solutions play an important role in practical application efficiency of these materials. One could assume that interactions of lignins with bound water and solutions depend strongly on the dispersion media and the presence of various (e.g., polar and ion-generating) solutes in water. The interfacial and temperature behaviors of water (solutions) bound to lignin particles in wetted powders could be effectively studied using low-temperature $^1$H NMR spectroscopy applied to static samples that allows one to separate mobile and immobile phases vs. temperature below freezing point ($T_{f,b}$) of bulk liquid. At $T < T_{f,b}$ several effects could be observed in wetted lignin powders such as confined space effects (CSE) in pores or voids between or inside crosslinked macromolecules, cryoscopic effects (CE) in bound solutions, partial freezing of liquids with cryoconcentration and differentiation of solutions, clusterization of bound liquids, etc. To elucidate some of these effects, wetted water-soluble lignin powders at a constant degree of hydration (h = 0.3 g/g) were studied in such dispersion media as air and chloroform-d alone or in a mixture with deuterated trifluoroacetic acid using the low-temperature $^1$H NMR spectroscopy method. Additionally, hydrated lignin molecules of different sizes were studied using quantum chemistry methods. Obtained results show that both CSE and CE affect the temperature behavior of bound water and related solutions. However, there is no their strong synergetic impact because the stronger bound the water (solution) the lower the activity of water as a solvent; i.e., CSE could partially inhibit CE. The obtained results are of interest in order to better understand different aspects of applications of water-soluble lignins under various conditions.*

***Keywords****: water-soluble lignin, bound water, interfacial phenomena, confined space effect, cryoscopic effect, dispersion media effect*

## INTRODUCTION

The transformation of lignin, which is one of the main biopolymers (as well as cellulose and hemicellulose), into valuable products is of importance from a practical point of view [1–8]. Industrial lignins (highly cross-linked hydrophobic water-insoluble polymers mainly composed of aromatic structures, primarily phenylpropanoids) are generated in great amounts as byproducts mainly in the pulp and paper production and biomass pretreatment processes [1–8]. The structure and characteristics of lignins [9–11] vary depending on source materials and industrial processes used [1–8]. Lignins composed of crosslinked macromolecules, typically insoluble in water, could be transformed into water-soluble materials (composed of smaller molecules with additionally attached polar functionalities and characterized by a smaller degree of crosslinking) using, *e.g.*, a sulfonation process [11–16]. Water-soluble lignins can be well dissolved in water at neutral or alkaline pH.

Lignin macromolecules have a lot of active O-containing functionalities [10, 11] that make it as a promising material for chemical modifications, *e.g.*, to prepare polymeric composites and other materials [11–21]. Lignin macromolecules contain both phenolic and aliphatic hydroxyls [10, 11], which can be used for additional functionalization to increase the range of lignin applications. Note that the ratio of the numbers of phenolic and aliphatic hydroxyls varies in lignins depending on the industrial processes. The phenolic hydroxyls as the most reactive functionalities can significantly affect the chemical reactivity of the lignin materials [1–11]. For example, to transform kraft lignin, it could be copolymerized with acrylic acid to produce a water-soluble lignin-based copolymer [22].

Water-soluble sulfuric acid lignin is a by-product of the acid saccharification of raw materials to produce biofuel [23, 24]. In various industries and technologies, water-soluble lignins have potential applications as dispersants, surfactants, bioplastics, additives, *etc*. [22–26]. As a whole, the behavior of water bound to water-soluble and water-insoluble lignins is of importance; therefore, this aspect is analyzed in the present study with respect to the water-soluble lignin.

The temperature and interfacial behaviors of water-soluble lignin in the wetted powders or aqueous media, as well as the behavior of water bound to lignin, are of importance since the related interfacial phenomena determine results of various applications of the materials. One of the effective methods to study the interfacial and temperature behaviors of bound water is the low-temperature $^1$H NMR spectroscopy and related cryoporometry applied to static samples to register mobile phases but not immobile ones [27–33]. The NMR spectroscopy is also effectively used to analyze the chemical structure of lignins [34–37]. Lignin interactions with water and solutions in different dispersion media (*e.g*., air, chloroform alone and with addition of ion-generating solutes such as trifluoroacetic acid $F_3CCOOD$, TFAA) studied here in detail using the $^1$H NMR spectroscopy are of interest for a deeper insight into the interfacial phenomena with the participation of hydrated lignins. The temperature range of 200–280 K used here allows us to analyze the behavior of bound (unfrozen at $T < 273$ K) water differently interacting with lignin macromolecules, solutes, and dispersion media. Under these conditions, there are strongly (SBW) and weakly (WBW) bound waters (unfrozen at $T < 265$ K and $265\ \text{K} < T < 273$ K, respectively) and strongly (SAW) and weakly (WAW) associated waters (with the chemical shift of the proton resonance $\delta_H = 4.0$–$5.5$ ppm and 0.5–2.0 ppm, respectively) [27]. In the case of low porosity of wetted materials, a fraction of water located out of pores could be assigned to unbound water (UBW) possessing the characteristics similar to those of free bulk water. It should be noted that the bulk aqueous solution of TFAA or dimethylsulfoxide (DMSO) demonstrates a complex dependence of the freezing temperature *vs.* solute concentration (Fig. 1) [38, 39] due to the colligative properties (cryoscopic effects) of the solution [33].

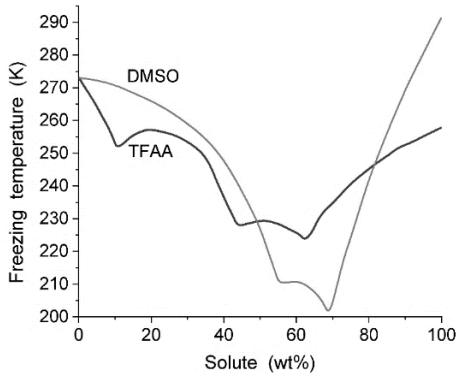


**Fig. 1.** Freezing temperature *vs*. solute (TFAA or DMSO) concentration in the aqueous solutions showing complex cryoscopic effects (due to the colligative properties of the solutions) resulting in the appearance of several eutectic points [38–40]

Note that similar temperature behaviors are observed for solutions with polar co-solvents (*e.g.*, alcohol and other deep eutectic solvents), dissolved and dissociated salts (NaCl, *etc*.), acids, and bases [38–47]. This behavior could be changed under the confined space effects in pores or in the interfacial layers at a solid surface out of pores. Note that nonpolar or weakly polar solvents (*e.g*., chloroform) immiscible with water do not lead to the cryoscopic effects (since the liquid phases are separated) in contrast to polar ones well mixed [48–58]. However, hydrophobic ones can change the interfacial and temperature behaviors and location of water bound to adsorbents to reduce the contact area between immiscible liquids that provides diminution of the Gibbs free energy of the system [27]. Note that hydrophilic and hydrophobic functionalities,

surface patches, and whole surface could provide different clusterization (organization) of bound water and solutes [27, 33, 59–62]. Therefore, one may expect that the temperature and interfacial behaviors and organization of water bound to the wetted lignin powder could depend strongly on the presence of TFAA (dissolved in water and water dissolved in TFAA that causes the cryoscopic effects affected by the chloroform medium) and water-immiscible chloroform that allows a deeper insight into the interfacial phenomena at a surface of wetted lignin particles. Elucidation of the mentioned aspects is the main aim of the present study.

## MATERIALS

Low molecular weight water-soluble (but insoluble in organic solvents) lignin as a brown lignosulfonate powder (Borregaard Lignotech, Sarpsborg), prepared using sulfite pulping process of hard/softwood as a precursor with a calcium/sodium blend, typically with 15 % ash removed, and the degree of sulfonation ~ 0.4, was used as received. Note that the sulfonation process introduces sulfonic acid groups into the lignin macromolecules. This results in the formation of water-soluble polymers, which can be used for various industrial applications. Microcellulose powder, MCP (Fluka) (see more details in [62]) was used for comparison with lignin. Deuterated chloroform, trifluoroacetic acid $F_3CCOOD$, and DMSO $(CD_3)_2SO$ (Merck, NMR spectroscopy grade) were used to avoid additional $^1H$ signals in the NMR spectra. Used water was bidistilled.

## METHODS

The low–temperature $^1H$ NMR spectra of static samples [27] with the wetted ($h = 0.3$ g water per gram of dry lignin) lignin powder were recorded using a Varian 400 Mercury spectrometer (magnetic field 9.4 T) utilizing 60° pulses of 1 μs duration. Each spectrum was recorded by co-addition of eight scans with a 2 s delay between each scan. Relative mean errors were less than ±10 % for $^1H$ NMR signal intensity for overlapped signals, and ±5 % for single signals (that are used for subsequent calculations of the amounts of unfrozen water $C_{uw}$ *vs*. $T$). Temperature control was accurate and precise to within ±1 K. The accuracy of integral intensities was improved by compensating for phase distortion and zero–line nonlinearity with the same intensity scale at different temperatures. To prevent supercooling, the spectra were recorded starting at 204–208 K for samples precooled to this temperature for 10 min. Samples were heated to 280 K at a rate of 5 K/min with steps $\Delta T = 2$–15 K, and maintained at a fixed temperature for 5 min for data acquisition at each temperature. Note that signals of immobile (frozen) small molecules and functionalities of macromolecules were not registered in the $^1H$ NMR spectra of static samples due to a narrow bandwidth (20 kHz) and a large difference in the transverse relaxation time of mobile and immobile phases (causing a large difference in their signal width) [27]. The spectra were recorded for samples (~0.2 g in NMR ampoules) located in different dispersion media such as air, $CDCl_3$ alone or with addition of $F_3CCOOD$ (6/1 v/v) (~2 ml).

Changes in the process of water freezing/melting are determined by a decrease in the Gibbs free energy ($\Delta G$) of water due to adsorption interactions in comparison to the bulk water [27]. This could be estimated from the equation for $\Delta G_{ice}$ *vs.* temperature for ice

$$\Delta G_{ice} = 0.0295 - 0.0413\Delta T + 6.64369\times10^{-5}(\Delta T)^2 + + 2.27708\times10^{-8}(\Delta T)^3 \text{ (kJ/mol)}, \quad (1)$$

where $\Delta T = 273.16 - T$ at 180 K < $T \le$ 273.15 K. The value of $\Delta G_s$ corresponds to maximal changes in the Gibbs free energy in the first adsorption layer. Changes in the Gibbs free energy of bound water *vs*. the amounts of unfrozen water ($C_{uw}$ in mg of water per gram of dry sample) were determined at $T = 204$–273 K [27] using tabulated $\Delta G(T)$ data for ice. The area under the $\Delta G(C_{uw})$ curve (obtained from the dependences of both $\Delta G$ and $C_{uw}$ on temperature) determines the surface Gibbs free energy $\gamma_S$ (the modulus of overall changes in the Gibbs free energy of bound water due to interaction with lignin) [27]

$$\gamma_S = -A \int_0^{C_{uw}^{max}} \Delta G(C_{uw}) dC_{uw}, \quad (2)$$

where $C_{uw}^{max}$ is the total amount of unfrozen water at $T = 273$ K, and $A$ (> 0) is a constant dependent on the type of units used in eq. (2). To take into account the amounts of unfrozen water bound in

the samples, the normalized (per gram of bound water) values $\gamma_S^* = \gamma_S/(C_{uw}^w + C_{uw}^s)$, where $C_{uw}^w$ and $C_{uw}^s$ are the amounts of weakly bound water, WBW (unfrozen at 265 K < $T$ < 273.15 K) and strongly bound water, SBW (unfrozen at $T$ < 265 K), respectively, were also computed.

Water can be frozen/melted in pores (or intramolecular voids in macromolecules and particles composed of lignin molecules) at lower temperatures ($T$ < 273 K) as described by the Gibbs–Thomson relation for the freezing/melting point depression for liquids confined in cylindrical pores of radius $R$ [27, 30–32]

$$\Delta T_m = T_{m,\infty} - T_m(R) = -\frac{2\sigma_{sl}T_{m,\infty}}{\Delta H_f \rho R} = \frac{k_{GT}}{R}, \qquad (3)$$

where $T_m(R)$ is the melting temperature of ice in cylindrical pores of radius $R$, $T_{m,\infty}$ the bulk melting temperature, $\Delta H_f$ the bulk enthalpy of fusion, ρ the density of the solid, $\sigma_{sl}$ the energy of solid-liquid interaction, and $k_{GT}$ is the Gibbs–Thomson constant (here $k_{GT}$ = 40 K nm). Eq. (3) was used to determine the cluster size distributions (CSD) or size distribution of pores (PSD) infilled by unfrozen water or solution ($f_V(R) = dV_{uw}(R)/dR$) at $T$ < 273 K [27]. The CSD (PSD) were converted into incremental CSD (ICSD, IPSD) $\Phi_V(R_i) = (f_V(R_{i+1}) + f_V(R_i))(R_{i+1} - R_i)/2$ at $\sum\Phi_{V,i}(R) = V_{uw}$. Integration of the $f_V(R)$ and $f_S(R)$ functions at 0.2 nm < $R$ < 1 nm, 1 nm < $R$ < 25 nm, and 25 nm < $R$ < 100 nm gives the volume and specific surface area of nano-, meso-, and macropores, respectively, contacted with unfrozen water (or aqueous solution). The specific surface area ($S_{uw}$) of lignin in contact with unfrozen bound water (assuming for simplicity that the density of this water $\rho_{uw}$ = 1 g/cm$^3$) can be determined from the amount of this water $C_{uw}^{max}$ (estimating pore volume as $V_{uw} = C_{uw}^{max}/\rho_{uw}$) at $T$ = 273.15 K and pore size distribution $f(R)$ with a model of cylindrical pores [27]

$$S_{uw} = \frac{V_{uw}}{2R_{av}} = \frac{2C_{uw}^{max}}{\rho_{uw}} \int_{R_{min}}^{R_{max}} f(R)dR \Big/ \int_{R_{min}}^{R_{max}} f(R)RdR, \qquad (4)$$

where $R_{min}$ and $R_{max}$ are the minimal and maximal radii of pores filled by unfrozen water, respectively [27]. The average melting temperature <$T_m$> was calculated as the ratio of the first and zero moments of the $C_{uw}(T)$ functions

$$< T_m >= \int_{T_{min}}^{T_0} TC_{uw}(T)dT \Big/ \int_{T_{min}}^{T_0} C_{uw}(T)dT, \qquad (5)$$

where $T_0$ = 273.15 K, and $T_{min}$ is the temperature corresponding to $C_{uw}$ = 0.

The chemical shift of the proton resonance ($\delta_H(T)$ function) depends on the number of possible configurations of the water molecules in the hydrogen bonds network (HBN) strongly affected not only by temperature but also by functionalized surroundings (*i.e.*, lignin molecules), solutes, co-solvents, and dispersion media [27, 63]. Considering that, this number is inversely proportional to the average number of the hydrogen bonds <$n_{HB}$>, according to the hydrogen bond network entropy definition $S \approx -k_B \ln n_{HB}$ [63]. Therefore, the temperature derivative of the measured fractional chemical shift

$$-\left(\frac{\partial \ln \delta(T)}{\partial T}\right)_p = -\left(\frac{\partial \ln < n_{HB} >}{\partial T}\right)_p \approx \left(\frac{\partial S}{\partial T}\right)_p \qquad (6)$$

should be proportional to the constant pressure specific heat $C_P(T)$ ($C_P = T(\partial S/\partial T)_P$). This aspect was analyzed in detail elsewhere [63]. One could assume that the function $s(T) = -T(\partial(\ln\delta(T))/\partial T)_P$ could demonstrate a different behavior for weakly (WAW) and strongly (SAW) associated waters, which are characterized by different $\delta_H$ values *vs.* $T$ [27]. Deuterated $CDCl_3$ and $CF_3COOD$ (D amounts > 99.9 %) were used upon the $^1$H NMR spectra recording to avoid signals from dispersion medium (and solute) used. Applications of the low-temperature $^1$H NMR spectroscopy and NMR cryoporometry methods to various materials were described in detail elsewhere [27, 64–69].

Quantum chemical calculations of water clusters using the density functional theory (DFT) method were carried out using a hybrid functional ωB97X–D with the cc–pVDZ basis set with the Gaussian 16 C.02 [70] or GAMESS 2023 R2 [71] program suits (Linux versions). The solvation effects were analyzed using the solvation method SMD [72] implemented in the Gaussian and GAMESS programs. To compute the Gibbs free energy of solvation (subscript s), $\Delta G_s = G_l - G_g$, where $G_l$ and $G_g$ are the Gibbs free energies of a molecule free or bound to silica cluster in the liquid (subscript l) and gas (g) media, respectively. The calculations were performed

taking into account zero-point and thermal corrections to the Gibbs free energy in the gas phase and for solved molecules and silica clusters with the geometry optimized using ωB97X–D/cc–pVDZ. The NMR spectra were calculated using the gauge-independent atomic orbital (GIAO) method calculated with or without the SMD method [70]. Large cluster models of water droplets and hydrated lignin molecules were calculated using the PM7 method (MOPAC, ver. 22.1, Linux) with (or without) the COSMO method to apply the solvation effects [73]. Preparation of initial cluster/molecular structures with water alone and hydrated lignin and visualization of the calculation results were carried out using several programs [74–77].

The distribution function of the $\delta_H$ values has been calculated with a simple equation [78]

$$f(\delta) = (2\pi\sigma^2)^{-0.5} \sum_j \frac{\exp[-(\delta_j - \delta)^2]}{2\sigma^2}, \qquad (7)$$

where $j$ is the number of H atom, $\sigma^2$ is the distribution dispersion, and $\delta_j$ is the value of chemical shift for $j$ atom and $\delta$ is the current value. The correlation equation $\delta_H = a + bq_H$ was used to estimate the $\delta_H$ values for water (or other compounds) in the large models computed with the PM7 method (to calculate the $q_H$ values). The equation constants $a$ and $b$ were estimated using the GIAO/ωB97X–D/cc–pVDZ method applied to a set of water clusters (20, 22, 44, and 100 $H_2O$ to calculate the $\delta_H$ values) and also calculated with the PM7 method (to obtain the $q_H$ values). An increase in a fraction of the H atoms participating in the hydrogen bonds with increasing size of water clusters and droplets (decreasing $S/V$ ratio for them) leads to reducing intensity of a band at $\delta_H$ = 1–3 ppm (WAW) and increasing one at $\delta_H$ = 4–6 ppm (SAW) (Fig. 2). At $n_{H2O} > 100$, the results change only slightly and the spectra are very similar at $n_{H2O} \geq 384$.

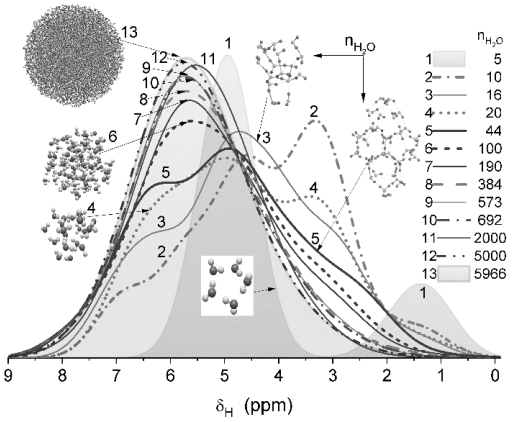


**Fig. 2.** $^1$H NMR spectra (normalized to unit) of water clusters and droplets of various sizes from $5H_2O$ to $5966H_2O$ computed using the GIAO/ωB97X–D/cc–pVDZ & PM7 correlation $\delta_H/q_H$ method (SAW is strongly predominant at $n_{H2O} \geq 100$)

## RESULTS AND DISCUSSION

The $^1$H NMR spectra of static samples with wetted lignin, located in different dispersion media (Fig. 3), and related computation results obtained with eqs. (1)–(6) (Figs. 4–6, Table 1) show the presence of water (and solutions) clusters and domains of various sizes and frozen at different temperatures. This assumption is confirmed by the presence of strongly (SAW) and weakly (WAW) associated waters, with signals registered in the spectra at $T < 273$ K. Signal intensity of strongly (unfrozen at $T < 265$ K) and weakly (unfrozen at 265 K < $T$ < 273 K) bound waters and unbound water (UBW frozen at temperature close to 273.15 K), as well as the SAW and WAW amounts, differently depend on temperature and system composition. Interactions of water with polar functionalities of lignin molecules and residual ash (undissolved or dissolved) and dissolved and dissociated TFAA result in a downfield shift of the SAW signals. Note that SBW is rather a poor solvent for any solute (including TFAA) [27]. Therefore, TFAA is mainly

dissolved in WBW/UBW/SAW, but a contribution of SBW increases due to TFAA dissolving in water (Figs. 3–6). Certain amounts of SAW and WAW are registered even at 204–208 K (Fig. 3) due to strong interactions of water with polar functionalities of lignin molecules and the presence of dissolved (in small amounts) polar low-molecular weight components (causing CE) of water-soluble lignin particles.

**Table 1.** Characteristics of unfrozen water at hydration degree $h$ = 0.3 g/g bound to lignin in different dispersion media

| Medium | Signal | $C_{uw}^{s}$ (mg/g) | $C_{uw}^{w}$ (mg/g) | $-\Delta G_s$ (kJ/mol) | $\gamma_S/\gamma_S^*$ (J/g) | $<T_m>$ (K) | $S_{nano,uw}$ ($m^2$/g) | $S_{meso,uw}$ ($m^2$/g) | $V_{nano,uw}$ ($cm^3$/g) | $V_{meso,uw}$ ($cm^3$/g) | $V_{macro,uw}$ ($cm^3$/g) |
|---|---|---|---|---|---|---|---|---|---|---|---|
| Air | 1 | 7.8 | 3.3 | 2.99 | 0.81/73.0 | 232.5 | 14.3 | 1.0 | 0.004 | 0.006 | 0 |
| Air | 2 | 0 | 36 | 0.45 | 0.33/9.2 | 269.5 | 0 | 2.8 | 0 | 0.026 | 0.274 |
| Air | 3+4 | 25 | 0.3 | 3.00 | 1.71/67.6 | 234.3 | 19.4 | 2.5 | 0.007 | 0.014 | 0.004 |
| $CDCl_3$ | 3 | 12 | 43 | 2.71 | 0.93/16.9 | 257.6 | 3.8 | 3.5 | 0.001 | 0.024 | 0.275 |
| +TFAA | 5 | 196 | 48 | 3.22 | 9.56/39.2 | 253.5 | 49 | 51 | 0.019 | 0.216 | 0.065 |

Note. $\gamma_S^* = \gamma_S/(C_{uw}^{w} + C_{uw}^{s})$ per gram of bound water ($\gamma_S$ is per gram of lignin). $\Delta G_s$ is the changes in the Gibbs free energy of the first adsorption layer ($S_{macro,uw} \approx 0$ for all samples)

Bound water and solutions are under the confined space effects in pores (voids) and the cryoscopic effects (in solutions), and both of them cause the freezing point depression (FPD) in parallel. Clearly, the results of CSE in lignin particles (in voids between macromolecules or in intramolecular voids in macromolecules physically or chemically crosslinked) and CE in the solutions (both leading to FPD) depend on dispersion media kind since it affects the organization of bound water and solutions at a surface of lignin particles. Note that the degree of lignin wetting is relatively low ($h$ = 0.3 g per gram of dry lignin). Therefore, wetted lignin remains in the powder state, and it could not be dissolved in chloroform (in amount of several times greater than the water amount) as a weakly polar solvent. As a whole, there are several $^1$H signals related to bound water (Fig. 3, signals 2 and 3) and aqueous solutions of low-molecular weight organics (signals 1 and 4). Signal 5 at ~8 ppm (Fig. 3 *e*, *f*) could be attributed to the aqueous solution of TFAA. The freezing point depression due to CE for the bulk mixture ($FPD_{CE,b}$) with consideration of the used amounts of water and TFAA could give $T_{f,b}$ = 225–230 K. However, significant decrease in signal intensity of water is observed at $T$ < 248 K (Fig. 3 *e*). This could be explained by incomplete mixing of water and TFAA (since some fraction of the latter could remain dissolved in chloroform) as well as by CSE inhibition of CE. In the lignin molecules, there are the H atoms in various bonds characterized by different $\delta_H$ values (*e.g.*, catechol at $\delta_H$ = 6.87 and 6.95 ppm, phenol 6.99 and 7.33 ppm, formic acid 8.47 ppm, *etc*.) [34]. Some fragments of macromolecules (as well as residual ash) having various bonds with H could be dissolved in SAW. This provides signals 1 (structures with the C–H bonds in alkyl functionalities) and 4 (H atoms in O-containing functionalities and aromatic structures as mentioned above).

The main fraction of water interacting with the lignin powder, located in air (Fig. 3 *a*) or $CDCl_3$ (Fig. 3 *c*) dispersion media, corresponds to WBW or unbound water since it frozen at $T$ close to 273 K. The presence of UBW is confirmed by condition $C_{uw}^{s} + C_{uw}^{w} < h$ for each sample studied (Table 1). This could be explained by several factors: (i) amount of water at $h$ = 0.3 g/g is too small to dissolve lignin particles, which remain as a wetted powder; (ii) lignin particles are weakly porous (*i.e.*, not all water could be located in pores/voids); (iii) swelling effect is insignificant (*i.e.*, small amount of bound water does not provide broadening of pores and increased porosity of the particles); (iv) as a whole, only a fraction of water is in contact with lignin molecules (a surface of lignin particles). Upon freezing-out (close to ~273 K) of a major fraction of UBW/WBW in the liquid phase, intensity of signals 1 and 4 only slightly decreases (after freezing of UBW) with decreasing temperature (Fig. 3 *b*, *d*) due to both CSE and colligative properties of the solutions of organics of low-molecular weights in a fraction of SAW. It should be noted that the lignin powder (immobile macromolecules) does not contribute the $^1$H NMR spectra of static samples due to measurement

conditions allowing recording the spectra of a mobile phase only.

Addition of TFAA strongly changes the temperature behavior of bound water/solution in comparison to samples located in air and $CDCl_3$ dispersion media (Figs. 3–6) due to the cryoscopic effect for the TFAA/water mixture (Fig. 1). For the used contents of water and TFAA, the freezing temperature of similar bulk solutions could be $T_{CE,b}$ = 225–230 K due to CE. However, only a small fraction of the solution is unfrozen at lower temperatures (Fig. 3 *e*, *f*) due to the CSE/CE for the bound TFAA solution with certain addition of other dissolved compounds (*e.g.*, formic acid, phenol, *etc*.) (Fig. 3 *d*). One may assume that CSE could partially inhibit CE. Therefore, the summarized CSE + CE do not prevent freezing-out of a significant fraction of the solution even at $T > T_{CE,b}$ since signal intensity diminution is observed already at 270 K < $T$ < 273 K in comparison to that at 280 K (Figs. 3 and 5 *a*). Thus, CSE partially inhibits CE since the stronger bound the solution the lower the activity of water as a solvent [27]. Note that the water/DMSO mixture bound to microcellulose (Fig. 3 *g*) demonstrates both CSE and CE, especially for water solution in DMSO (signal at $\delta_H$ = 3.0–3.5 ppm). The CSE+CE influence on water/DMSO is stronger than that on water/TFAA bound to the lignin powder due to several factors: (i) CE for the bulk solution is stronger for the former at $C_{DMSO}$ = 50–85 wt. % (Fig. 1); (ii) MCP has $S_{uw}$ up to 250 $m^2/g$ [62], which is several times larger than that for the lignin systems (Table 1) because MCP is composed of linear polysaccharides (with β(1→4) linked D-glucose units) more hydrophilic than crosslinked lignin macromolecules including aromatic functionalities. Water (DMSO-free) bound to MCP is practically completely frozen at $T$ < 220 K (Fig. 3 *g*, signal at $\delta$ = 4–5 ppm) in contrast to water mixed with DMSO (3.0–3.5 ppm) due to the CE influence similar to CE for water/TFAA bound to lignin. Note that the freezing point depression due to CE for the used amounts of water and DMSO (in bulk) corresponds to $T_{f,b}$ = 245 K (Fig. 1). However, not all water interacts with DMSO (Fig. 3 *g*). Additionally, a fraction of DMSO could be dissolved in chloroform with no contacts with water, and the CSE could inhibits CE. All these effects could lead to greater $FPD_{CE}$ for the mixture. Thus, aromatic functionalities and crosslinking of lignin macromolecules could inhibit strong interactions with water and aqueous solutions. Therefore, the dual hydrophobic/hydrophilic nature of lignins should be considered upon practical applications of these materials.

The value of $S_{uw} = S_{nano,uw} + S_{meso,uw}$ ($S_{macro,uw} \approx 0$ for all samples studied since water in macropores mainly corresponds to UBW with no direct contact to a surface of lignin particles) is equal to 40 $m^2/g$ for a sample located in air (Table 1). For chloroform as a dispersion medium, this value is much smaller because chloroform can displace water from pores onto the outer surface or into macropores of lignin particles ($V_{nano,uw}$, $V_{meso,uw}$, and SBW decrease but $V_{macro,uw}$ and WBW/UBW increase) (Figs. 5 and 6) to reduce the contact area between immiscible liquids. The $S_{uw}$ and $V_{meso,uw}$ values increase with addition of TFAA (Table 1, Fig. 5). However, it is possible certain overestimation of these values (as well as $-\Delta G_s$ and $\gamma$, Table 1) due to the colligative properties of the acidic solution; *i.e.*, eq. (3) should be corrected, *e.g.*, $\Delta T_{f,CSE} - \alpha \Delta T_{f,CE/CSE} = -k/R$, where $\alpha < 1$ for miscible compounds (*e.g.*, TFAA + water) and $\alpha = 0$ for immiscible ones (*e.g.*, water + chloroform). The $<T_m>$ value (Table 1) is minimal for signals 1 and 4 attributed to the solutions of small organic molecules mobile due to dissolution in SAW/UBW. For the TFAA solution in SAW/UBW/WBW, the $<T_m>$ value decreases in comparison to signal 2 (in air) and signal 3 (in chloroform) due to the cryoscopic effects.

The chemical shifts $\delta_H$ related to different signals in mobile phases with bound water and solutions depend on temperature (Fig. 4 *a*). This effect (as well as changes in other characteristics, Figs. 5 and 6) could be explained by several factors: (i) freezing-out (or melting) of UBW at $T$ close to 273 K, then WBW (up to 265 K) and finally SBW ($T$ = 204–265 K); (ii) effects of the dispersion media (air *vs*. chloroform); (iii) effects of solutes (TFAA and low-molecular weight fragments of lignin (including ash) and residual amounts of reagents used on lignin preparation); (iv) reorganization of unfrozen water upon freezing-out of a water fraction due to larger volume of ice than liquid water and changes in structure of pores (voids) infilled by unfrozen and frozen water or solutions. Therefore, the $\delta_H(T)$

functions are nonmonotonic (Fig. 4 *a*) due to the mentioned effects. These effects also cause the appearance of some extrema of the *s*(*T*) function (Fig. 4 *b*) related to changes in the entropy of the hydrogen bond network. The maximal changes in this function are observed at temperatures close to 270–273 K since melting/freezing of SAW/UBW/WBW, providing predominant contribution to total amount of water/solutions, occurs in this temperature range.

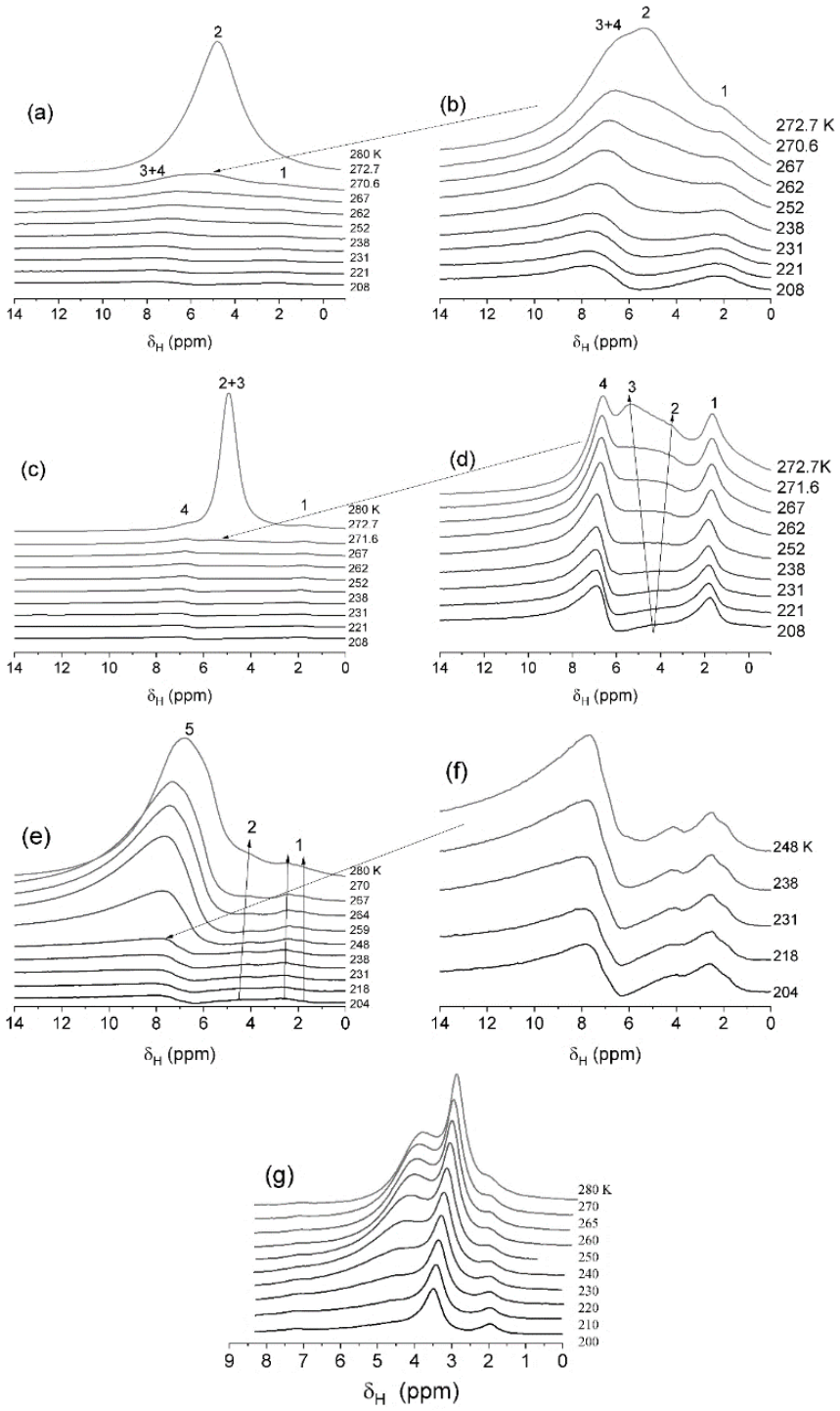


**Fig. 3.** $^{1}$H NMR spectra of water (0.3 g/g)/lignin in different dispersion media: (*a*, *b*) air, (*c*, *d*) chloroform-d, and (*e*, *f*) 6$CDCl_3$+1TFAA; the right column (*b*, *d*, *f*) shows the spectra only at lower temperatures for a better view; (*g*) wetted microcellulose powder ($h$ = 0.14 g/g) located in $CDCl_3$ medium with addition of DMSO (0.7 g/g): $\delta_H$ = 3.0–3.5 ppm (water/DMSO), 2 ppm (residual DMSO with attached H), and 4–5 ppm (bound water)

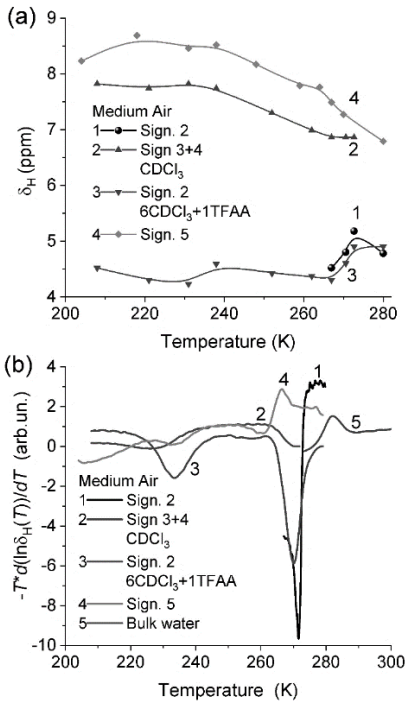


**Fig. 4.** (*a*) The chemical shifts $\delta_H$(T) of bound water as a function of temperature for selected signals (see Fig. 3); and (*b*) function $s(T) = -T(\partial(\ln\delta(T))/\partial T)_P$ *vs.* temperature for the same lines as in (*a*) (with no signal 1 of too low intensity)

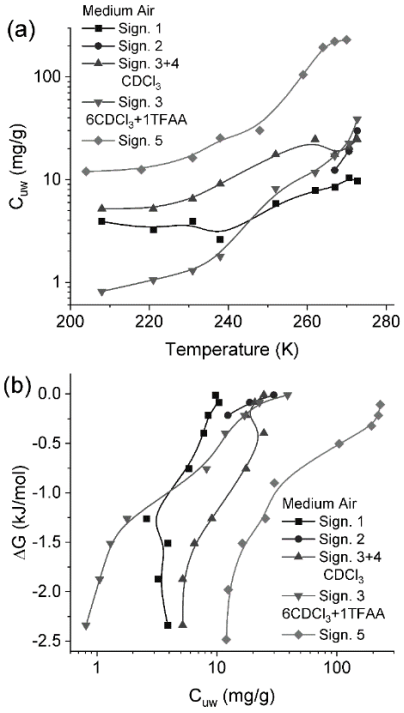


**Fig. 5.** (*a*) The amounts of unfrozen water $C_{uw}(T)$ *vs.* temperature for selected signals (see Fig. 3) and (*b*) the relations between $C_{uw}(T)$ and changes in the Gibbs free energy of water due to the interactions with lignin

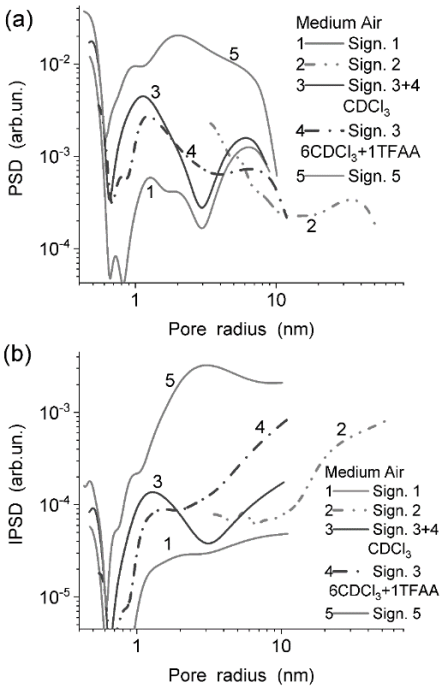


**Fig. 6.** The size distributions of pores infilled by unfrozen water for selected signals (see Fig. 3) as (*a*) differential and (*d*) incremental distribution functions (high intensity of PSD for water/solution responsible for signal 5 is due to CE for water/TFAA)

Minimal changes in $C_{uw}$ *vs*. $T$ (Fig. 5 *a*) and $\Delta G$ *vs*. $C_{uw}$ (Fig. 5 *b*) are observed for signals 1 and 4 (in air) because of contribution of solutions of polar organics (dissolved in SAW/WBW/UBW) and the cryoscopic effects, as well as CSE. In the chloroform dispersion medium, the $C_{uw}^{s}$ value decreases (Table 1, Fig. 5 *a*). However, addition of TFAA gives the opposite result. The changes in the unfrozen water organization are well observed in the courses of the PSD/IPSD functions for different signals (*i.e.*, different water/solution structures) (Fig. 6) related to the size distributions of pores (voids) infilled by unfrozen water or solutions.

Minimal pore (cluster) sizes with minimal intensity of PSD/IPSD (Fig. 6 *a*, *b*, curves 1) correspond to a solution responsible for signal 1 (Fig. 3 *a*, *b*). Signal 2 is linked to clusters and domains of maximal sizes with small intensity especially for PSD (Fig. 6, curves 2, up to 50 nm in radius), which could be attributed to WBW/SAW. Signal 3 corresponds to decreased contribution of smaller structures ($R$ < 3 nm) and increased contribution of larger ones ($R$ > 3 nm) in the chloroform medium (Fig. 6, curves 4) in comparison to air (curves 3). Signal 5 (Fig. 6, curves 5) related to the TFAA solution corresponds to maximal contributions over a broad range of pores due to both confined space and cryoscopic effects. Note that the PSD/IPSD at $R$ > 10 nm is only for signal 2 (WBW/SAW and UBW). The structures responsible for other signals are characterized by PSD/IPSD at $R$ < 10 nm (Fig. 6). Therefore, bound water and solutions at $h$ = 0.3 g/g are mainly located in nanopores and narrow mesopores in lignin particles.

The theoretical calculations show that dry and wetted lignin molecules have different $^{1}$H spectra (Fig. 7). Strongly hydrated lignin molecule ($h$ = 1.015 g/g) has a spectrum mainly depending on bound water. It is slightly broadened in comparison to a spectrum of only bound water. However, an experimental spectrum is broadened in comparison to the theoretical ones due to more complex structure of real lignin macromolecules and particles. A decrease in the hydration degree ($h$ = 0.471 g/g) of twice smaller lignin molecule (Fig. 7, curves 4 and 5) results in a certain upfield shift (PM7) and downfield shift (DFT) of the spectrum. This is due to the difference in the water shell organization since the DFT method gives a denser water shell than PM7 does (vide infra). Note that the GIAO/DFT method gives the spectrum of bound water (curve 5) closer to the experimental one (curve 6) than PM7 gives (curve 4).

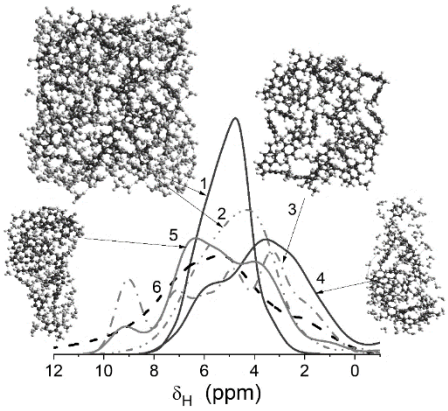


**Fig. 7.** Theoretical calculations of the $^{1}$H NMR spectra of lignin molecule (762 atoms, 5556.52 Da) hydrated by 313 $H_2O$ ($h$ = 1.015 g/g): (curve 1) only water molecules, (2) total spectrum of lignin/water, (3) only lignin, (4 and 5) water ($h$ = 0.471 g/g, 72 $H_2O$) bound to a smaller molecule (378 atoms, 2753.13 Da) calculated with PM7 (4) and GIAO/ωB97X–D/cc–pVDZ (5), and (6) experimental spectrum of water bound to lignin in air at 272.7 K (upper spectrum in Fig. 3b) (for better view, all spectra are normalized to unit)

Individual small molecules alone do not provide the porous structure characteristic for dry (or weakly wetted) lignin particles or macromolecules. The porosity (providing the confined space effects) plays an important role in the organization of bound water. However, in the case of larger molecular model of lignin, there are intramolecular voids infilled by water in contrast

to a smaller model (Fig. 7, inserts). This difference explains the upfield shift of the spectrum of water bound to smaller molecule (Fig. 7, curve 4) in comparison to larger one (curve 1) calculate by the PM7 method. Note that the interaction energy between the lignin molecule (smaller model) and water shell is equal to –20.4 kJ/mol (PM7) and –30.2 kJ/mol (DFT) per water molecule. Consequently, this molecular model of lignin corresponds to hydrophilic one, despite the interaction energy between water molecules in the water shell is stronger as –33.3 kJ/mol (PM7) and –45.5 kJ/mol (DFT) per molecule. However, this difference explains the absence of complete water spreading on the surface of wetted lignin particles, since bound water tends to form large clusters and domains out of pores in lignin particles, and according to $^1$H NMR spectra (Fig. 3), this water is freezing-out at temperature close to 273 K.

## CONCLUSION

Conversion of lignins as byproducts of different origin into various valuable products is of importance from a practical point of view. One of the corresponding pathways is the preparation of water-soluble lignins, for which interactions with water and aqueous solutions play an important role in efficiency of the material applications. One could assume that interactions of any lignin with water and solutions depend strongly on the dispersion media and the presence of various (*e.g.*, polar and ion-generating) solutes in water. The interfacial and temperature behaviors of water (solutions) bound to lignin particles in wetted powders could be effectively studied using low-temperature $^1$H NMR spectroscopy of static samples that allows one to separate mobile and immobile phases *vs*. temperature below freezing point $T_{f,b}$ of a bulk liquid. At $T < T_{f,b}$ several effects could be observed in the wetted lignin powder such as the confined space effects in pores or voids between or inside 3D-branched crosslinked macromolecules, cryoscopic effects in solutions, partial freezing of liquids, cryoconcentration and differentiation of solutions, clusterization of bound liquids, *etc*. To elucidate some of these effects, wetted lignin (water-soluble) at constant degree of hydration ($h$ = 0.3 g/g) was studied in air and chloroform-d alone and in mixture with deuterated trifluoroacetic acid using the $^1$H NMR spectroscopy applied to static samples. Additionally, hydrated lignin molecules were modeled using quantum chemistry methods. Obtained experimental results show that both CSE and CE affect the temperature behavior of bound water and related solutions depending on the system composition. However, there is no their synergetic effect because the stronger bound the water (solution) the lower the activity of water as a solvent; *i.e.*, CSE could partially inhibit CE. Therefore, the amounts of unfrozen solutions bound to lignin particles at $T < T_{CE,b} \approx 230$ K are much smaller (< 0.02 g/g) even with the presence of TFAA than the total amount of water used (0.3 g/g). The obtained results allow one a deeper insight into a problem of interactions of water-soluble lignin molecules and particles with various environment that is of importance for applications of the materials. In future, it could be interesting to study water-soluble lignin over a broad range of hydration up to its completely dissolution in the aqueous media.

## ACKNOWLEDGEMENTS

The authors are grateful to the National Research Foundation of Ukraine (Support of advanced and young scientists, grant 2020.02/0057) for financial support of this study. V.M.G. is grateful to Gaussian, Inc. for the Gaussian 16, Revision C.02 program suit. The authors thank Dr. O. Sevastyanova (KTH Royal Institute of Technology, Stockholm) for water-soluble lignin sample.

# Міжфазна та температурна поведінка води та розчинів, що зв'язані у порошку водорозчинного лігніну

**В.М. Гунько, В.В. Туров**

*Інститут хімії поверхні ім. О.О. Чуйка Національної академії наук України*
*вул. Генерала Наумова, 17, Київ, 03164, Україна, vlad_gunko@ukr.net*

*Перетворення лігнінів різного походження на цінні продукти є важливим з практичної точки зору. Одним із відповідних шляхів є отримання водорозчинних лігнінів, для яких взаємодія з водою та водними розчинами відіграє важливу роль в ефективності практичного застосування цих матеріалів. Можна припустити, що взаємодія лігнінів з водою та розчинами сильно залежить від дисперсійних середовищ і присутності різноманітних (наприклад, полярних та іоногенеруючих) розчинених речовин у воді. Міжфазну та температурну поведінку води (розчинів), зв'язаної з частинками лігніну у зволожених порошках, можна ефективно досліджувати за допомогою низькотемпературної $^1$H ЯМР-спектроскопії статичних зразків, що дозволяє розділити рухливі та нерухомі фази в залежності від температури нижче точки замерзання ($T_f$) рідини. При $T < T_f$ у вологих зразках порошку можна спостерігати кілька ефектів, таких як ефекти обмеженого простору (CSE) у порах або порожнечах між або всередині макромолекул, кріоскопічні ефекти (CE) у розчинах, часткове заморожування рідин, кріоконцентрація та диференціація розчинів, кластеризація зв'язаних рідин тощо. Щоб з'ясувати деякі з цих ефектів, змочений лігнін (водорозчинний) при постійному ступені гідратації (h = 0.3 г/г) досліджували на повітрі та хлороформі-d окремо та в суміші з дейтерованою трифторацтовою кислотою з використанням методу $^1$H ЯМР, застосованого до статичних зразків. Крім того, методами квантової хімії досліджували гідратовані молекули лігніну. Отримані результати показують, що як CSE, так і CE впливають на температурну поведінку зв'язаної води та пов'язаних розчинів. Однак їхній синергетичний ефект відсутній, тому що чим міцніше зв'язана вода (розчин), тим нижча активність води як розчинника; тобто, CSE може частково пригнічувати CE. Отримані результати становлять інтерес з практичної точки зору для застосування водорозчинних лігнінів.*

***Ключові слова**: водорозчинний лігнін, зв'язана вода, міжфазні явища, ефекти обмеженого простору, кріоскопічні ефекти, ефект дисперсійного середовища*

REFERENCES

1. *Ullmann's Encyclopedia of Industrial Chemistry*. (Weinheim: Wiley–VCH, 2007).
2. *Kirk–Othmer Encyclopedia of Chemical Technology*. (John Wiley & Sons, Inc. 2001).
3. Sjöström E. *Wood Chemistry: Fundamentals and Applications*. Second ed. (Academic Press. 1993).
4. Rehman A., Nazir G., Heo K., Hussain S., Ikram M., Akhter Z., Algaradah M.M., Mahmood Q., Fouda A.M. A focused review on lignocellulosic biomass-derived porous carbons for effective pharmaceuticals removal: Current trends, challenges and future prospects. *Sep. Purif. Technol*. 2024. **330**: 125356.
5. Afraz M., Muhammad F., Nisar J., Shah A., Munir S., Ali G., Ahmad A. Production of value added products from biomass waste by pyrolysis: An updated review. *Waste Management Bulletin*. 2024. **1**: 30.
6. Radoor S., Karayil J., Jayakumar A., Kandel D.R., Kim J.T., Siengchin S., Lee J. Recent advances in cellulose- and alginate-based hydrogels for water and wastewater treatment: A review. *Carbohydr. Polym.* 2024. **323**: 121339.
7. Sahraeian S., Rashidinejad A., Golmakani M.-T. Recent advances in the conjugation approaches for enhancing the bioavailability of polyphenols. *Food Hydrocolloids.* 2024. **146**: 109221.
8. Mennani M., Kasbaji M., Benhamou A.A., Boussetta A., Kassab Z., El Achaby M., Grimi N., Moubarik A. The potential of lignin-functionalized metal catalysts - A systematic review. *Renewable Sustainable Energy Rev.* 2024. **189**: 113936.
9. Jones I.D., Smol J.P. (editors). *Wetzel's Limnology. Lake and River Ecosystems*. 4th Edition. (Academic Press: Oxford, 2023).
10. Davin L.B., Lewis N.G. Lignin primary structures and dirigent sites. *Curr. Opin. Biotechnol*. 2005. **16**(4): 407.
11. Heitner C., Dimmel D.R., Schmidt J.A. (editors). *Lignin and Lignans. Advances in Chemistry*. (Boca Raton: CRC Press, 2010).
12. Savy D., Cozzolino V., Vinci G., Nebbioso A., Piccolo A. Water-soluble lignins from different bioenergy crops stimulate the early development of maize (*Zea mays*, L.). *Molecules.* 2015. **20**(11): 19958.

13. Tian D., Zhang J., Hu J., Huang M., Zhao L., Lei Y., Zou J., Zhang S., Shen F. A new water-soluble lignin incorporation enhanced the barrier performance of liquid mulching film. *Chem. Eng. J.* 2023. **452**: 139383.
14. Zhang Y., Ren H., Maarof H., Udin S.M., Liu Y., Li M., Alias H., Duan E. The effect of water content on lignin solubilization in deep eutectic solvents. *J. Mol. Liq.* 2023. **374**: 121271.
15. Wang R., Zheng L., Xu Q., Xu L., Wang D., Li J., Lu G., Huang C., Wang Y. Unveiling the structural properties of water–soluble lignin from gramineous biomass by autohydrolysis and its functionality as a bioactivator (anti–inflammatory and antioxidative). *Inter. J. Bio. Macromol*. 2021. **191**: 1087.
16. Lai C.-Y., Sun Y.-M., Liu Y.-L. Water-soluble ozonated lignin as a hydrophilic modifier for poly(vinyl alcohol) membranes for pervaporation desalination. *J. Membrane Sci.* 2023. **685**: 121959.
17. Bajwa D.S., Pourhashem G., Ullah A.H., Bajwa S.G. A concise review of current lignin production, applications, products and their environmental impact. *Ind. Crops Prod*. 2019. **139**: 111526.
18. Hodásová Ľ., Jablonský M., Škulcová A., Ház A. Lignin, potential products and their market value. *Wood Res*. 2015. **60**(6): 973.
19. Budnyak T.M., Piątek J., Pylypchuk I.V., Klimpel M., Sevastyanova O., Lindström M., Gun'ko V.M., Slabon A. Membrane–filtered kraft lignin–silica hybrids as bio-based sorbents for cobalt(ii) ion recycling. *ACS Omega*. 2020. **5**(19): 10847.
20. Zhou N., Thilakarathna W.P.D.W., He Q.S., Rupasinghe H.P.V. A review: Depolymerization of lignin to generate high-value bio-products: Opportunities, challenges, and prospects. *Front. Energy Res.* 2022. **9**: 758744.
21. Xu Z., Lei P., Zhai R., Wen Z., Jin M. Recent advances in lignin valorization with bacterial cultures: microorganisms, metabolic pathways, and bio-products. *Biotechnol. Biofuels*. 2019. **12** :32.
22. Kong F., Wang S., Price J.T., Konduri M.K.R., Fatehi P. Water soluble kraft lignin–acrylic acid copolymer: synthesis and characterization. *Green Chem*. 2015. **17**(8): 4355.
23. Ohara T., Yuasa K., Kimura K., Komaki S., Nishina Y., Matsukawa A. A novel mechanical plant compression system for biomass fuel and acquisition of squeezed liquid with water-soluble lignin as anti-virus materials. *J. Mater. Cycles Waste Manag*. 2023. **25**: 249.
24. Xu C., Ferdosian F. *Conversion of Lignin into Bio-Based Chemicals and Materials. Green Chemistry and Sustainable Technology.* (Berlin: Springer, 2017).
25. Wang H., Pu Y., Ragauskas A., Yang B. From lignin to valuable products–strategies, challenges, and prospects. *Bioresource Technology*. 2019. **271**: 449.
26. Liu Q., Matsushita Y., Aoki D., Fukushima K. Industrial utilizations of water-soluble sulfuric acid lignin prepared by hydrothermal treatment as flocculant and dispersant. *J. Wood Sci*. 2019. **65**: 18.
27. Gun'ko V.M., Turov V.V. *Nuclear Magnetic Resonance Studies of Interfacial Phenomena*. (Boca Raton: CRC Press, 2013).
28. Franks F. *Biophysics and Biochemistry at Low Temperatures*. (Cambridge: Cambridge University Press. 1985).
29. Grout B.W.W., Morris G.J. (editors). *The Effects of Low Temperatures on Biological Systems*. (London: Edward and Arnold Publishers. 1987).
30. Kimmich R. *NMR Tomography, Diffusometry, Relaxometry*. (Heidelberg: Springer, 1997).
31. Petrov O.V., Furó I. NMR cryoporometry: Principles, applications and potential. *Prog. Nuclear Magn. Reson. Spectr*. 2009. **54**(2): 97.
32. Mitchell J., Webber J.B.W., Strange J.H. Nuclear magnetic resonance cryoporometry. *Phys. Rep*. 2008. **461**(1): 1.
33. Chaplin M. *Water structure and science*. http://www1.lsbu.ac.uk/water/, accessed on 2 October, 2023.
34. Halleraker H.V., Barth T. Quantitative NMR analysis of the aqueous phase from hydrothermal liquefaction of lignin. *J. Anal. Appl. Pyrolysis*. 2020. **151**: 104919.
35. Zhang L., Yan L., Wang Z., Laskar D.D., Swita M.S., Cort J.R., Yang B. Characterization of lignin derived from water–only and dilute acid flowthrough pretreatment of poplar wood at elevated temperatures. *Biotechnol. Biofuels.* 2015. **8**: 203.
36. Pylypchuk I.V., Lindén P.A., Lindström M.E., Sevastyanova O. New insight into the surface structure of lignin nanoparticles revealed by $^{1}$H liquid–state NMR spectroscopy. *ACS Sustainable Chem. Eng.* 2020. **8**(36): 13805.
37. Burger R., Lindner S., Rumpf J., Do X.T., Diehl B.W.K., Rehahn M., Monakhova Y.B., Schulze M. Benchtop versus high field NMR: Comparable performance found for the molecular weight determination of lignin. *J. Pharm. Biomed. Anal*. 2022. **212**: 114649.
38. Harriss M.G., Milne J.B. The trifluoroacetic acid solvent system. Part V. Cryoscopic measurements. *Can. J. Chem*. 1976. **54**(19): 3031.
39. Cady H.H., Cady G.H. Freezing points of the system water–trifluoroacetic acid. *J. Am. Chem. Soc*. 1954. **76**(3): 915.
40. Rasmussen D.H., MacKenzie A.P. Phase diagram for the system water–dimethylsulphoxide. *Nature*. 1968. **220**: 1315.
41. *Technical Bulletin Reaction Solvent Dimethyl Sulfoxide* (105B DMSO). Gaylord Chemical. 2011. 105FINALnoframe2.doc (chemistry–chemists.com).
42. Lam S.Y., Benoit R.L. Some thermodynamic properties of the dimethylsulfoxide–water and propylene carbonate–water systems at 25 °C. *Can. J. Chem*. 1974. **52**(5): 718.

43. Lü P., Zhao G., Zhang X., Yin J., Bao J. Measurement and prediction on the surface properties of dimethyl sulfoxide/water mixtures. *Chem. Res. Chin. Univ.* 2016. **32**: 100.
44. Mohan G., Venkataraman M., Gomez-Vidal J., Coventry J. Assessment of a novel ternary eutectic chloride salt for next generation high-temperature sensible heat storage. *Energy Convers. Manage*. 2018. **167**: 156.
45. Viola W., Andrew T.L. An aqueous eutectic electrolyte for low-cost, safe energy storage with an operational temperature range of 150 °C, from –70 to 80 °C. *J. Phys. Chem. C*. 2021. **125**(1): 246.
46. Barnes W.H., Maass O. Freezing points and heat capacities of aqueous solutions of potassium chloride. *Can. J. Res.* 1930. **2**(3): 218.
47. Haghighi H., Chapoy A., Tohidi B. Freezing point depression of electrolyte solutions: experimental measurements and modeling using the cubic–plus–association equation of state. *Ind. Eng. Chem. Res*. 2008. **47**(11): 3983.
48. Kamide K. Colligative properties. *Comprehensive Polymer Science and Supplements*. 1989. **4**: 75.
49. Kamide K., Dobashi T. *Physical Chemistry of Polymer Solutions. Theoretical Background*. (Elsevier, 2000).
50. Reuter J.H., Perdue E.M. Calculation of molecular weights of humic substances from colligative data: Application to aquatic humus and its molecular fractions. *Geochim. Cosmochim. Acta.* 1981. **45**(11): 2017.
51. Stepanos J.J., Addison A.W. *Chemical Thermodynamics and Statistical Aspects: Questions to Ask in Fundamentals and Principle*. (Elsevier, 2023).
52. Mazza D., Canuto E. *Fundamental Chemistry with Matlab*. (Elsevier, 2022).
53. Gaffney J.S., Marley N.A. *General Chemistry for Engineers*. (Elsevier, 2018).
54. DeVoe H. *Thermodynamics and Chemistry, LibreTexts, Chemistry*. (California State University, 2022).
55. Pancerz M., Ptaszek A., Sofińska K., Barbasz J., Szlachcic P., Kucharek M., Łukasiewicz M. Colligative and hydrodynamic properties of aqueous solutions of pectin from cornelian cherry and commercial apple pectin. *Food Hydrocolloids.* 2019. **89**: 406.
56. Gonda I., Groom C. V. Colligative properties of disodium cromoglycate aqueous solutions in relation to their phase diagram. *J. Colloid Interface Sci*. 1983. **92**: 289.
57. Nagvekar M., Tihminlioglu F., Danner R.P. Colligative properties of polyelectrolyte solutions. *Fluid Phase Equilib*. 1998. **145**(1): 15.
58. Mjallal I., Feghali E., Hammoud M., Habchi C., Lemenand T. Exploring the colligative properties of Arachidic acid for potential use as PCM. *Solar Energy.* 2021. **214**: 19.
59. Gun'ko V.M., Turov V.V., Zarko V.I., Dudnik V.V., Tischenko V.A., Voronin E.F., Kazakova O.A., Silchenko S.S., Barvinchenko V.N., Chuiko A.A. Aqueous suspensions of fumed silica and adsorption of proteins. *J. Colloid Interface Sci.* 1997. **192**(1): 166.
60. Gun'ko V.M., Voronin E.F., Zarko V.I., Goncharuk E.V., Turov V.V., Pakhovchishin S.V., Pakhlov E.M., Guzenko N.V., Leboda R., Skubiszewska-Zięba J., Janusz W., Chibowski S., Chibowski E., Chuiko A.A. Interaction of poly(vinyl pyrrolidone) with fumed silica in dry and wet powders and aqueous suspensions. *Colloids Surf. A.* 2004. **233**(1–3): 63.
61. Mironyuk I.F., Gun'ko V.M., Vasylyeva H.V., Goncharuk O.V., Tatarchuk T., Mandzyuk V.I., Bezruka N.A., Dmytrotsa T.V. Effects of enhanced clusterization of water at a surface of partially silylated nanosilica on adsorption of cations and anions from aqueous media. *Microporous Mesoporous Mater*. 2019. **277**: 95.
62. Turov V.V., Gun'ko V.M., Barvinchenko V.N., Rugal A.A., Turova A.A., Fedyanina V.V., Hydration of cellulose with the presence of quercetin and organic solvents. *Chemistry, Physics, and Technology of Surface*. 2009. **15**: 169.
63. Mallamace F., Corsaro C., Broccio M., Branca C., González–Segredo N., Spooren J., Chen S.–H. Stanley H.E. NMR evidence of a sharp change in a measure of local order in deeply supercooled confined water. *Proc. Natl. Acad. Sci. USA*. 2008. **105**(35): 12725.
64. Gun'ko V.M., Turov V.V., Krupska T.V., Borysenko M.V. Surroundings effects on the interfacial and temperature behaviors of NaOH/water bound to hydrophilic and hydrophobic nanosilicas. *J. Colloid Interface Sci*. 2023. **634**: 93.
65. Gun'ko V.M., Turov V.V., Pakhlov E.M., Krupska T.V., Charmas B. Effect of water content on the characteristics of hydro–compacted nanosilica. *Appl. Surf. Sci*. 2018. **459**: 171.
66. Gun'ko V.M., Turov V.V., Goncharuk O.V., Pakhlov E.M., Matkovsky O.K. Interfacial phenomena at a surface of individual and complex fumed nanooxides. *Surface*. 2019. **11(26)**: 3.
67. Gun'ko V.M., Turov V.V., Zarko V.I., Goncharuk E.V., Gerashchenko I.I., Turova A.A., Mironyuk I.F., Leboda R., Skubiszewska–Zięba J., Janusz W. Comparative characterization of polymethylsiloxane hydrogel and silylated fumed silica and silica gel. *J. Colloid Interface Sci*. 2007. **308**(1): 142.
68. Gun'ko V.M., Turov V.V., Krupska T.V., Protsak I.S., Borysenko M.V., Pakhlov E.M. Polymethylsiloxane alone and in composition with nanosilica under various conditions. *J. Colloid Interface Sci*. 2019. **541**: 213.
69. Gun'ko V.M., Turov V.V. Nanostructured systems based on polymethylsiloxane and nanosilicas with hydrophobic and hydrophilic functionalities. *Colloids Surf. A*. 2023. **677**: 132448.
70. Frisch M.J., Trucks G.W., Schlegel H.B., Scuseria G.E., Robb M.A., Cheeseman J.R., Scalmani G., Barone V., Petersson G.A., Nakatsuji H., Li X., Caricato M., Marenich A.V., Bloino J., Janesko B.G., Gomperts R., Mennucci B.,

Hratchian H.P., Ortiz J.V., Izmaylov A.F., Sonnenberg J.L., Williams–Young D., Ding F., Lipparini F., Egidi F., Goings J., Peng B., Petrone A., Henderson T., Ranasinghe D., Zakrzewski V.G., Gao J., Rega N., Zheng G., Liang W., Hada M., Ehara M., Toyota K., Fukuda R., Hasegawa J., Ishida M., Nakajima T., Honda Y., Kitao O., Nakai H., Vreven T., Throssell K., Montgomery J.A. Jr., Peralta J.E., Ogliaro F., Bearpark M.J., Heyd J.J., Brothers E.N., Kudin K.N., Staroverov V.N., Keith T.A., Kobayashi R., Normand J., Raghavachari K., Rendell A.P., Burant J.C., Iyengar S.S., Tomasi J., Cossi M., Millam J.M., Klene M., Adamo C., Cammi R., Ochterski J.W., Martin R.L., Morokuma K., Farkas O., Foresman J.B., Fox D.J. *Gaussian 16, Revision C.02*. (Gaussian, Inc., Wallingford CT, 2019).

71. Barca G.M.J., Bertoni C., Carrington L., Datta D., De Silva N., Deustua J.E., Fedorov D.G., Gour J.R., Gunina A.O., Guidez E., Harville T., Irle S., Ivanic J., Kowalski K., Leang S.S., Li H., Li W., Lutz J.J., Magoulas I., Mato J., Mironov V., Nakata H., Pham B.Q., Piecuch P., Poole D., Pruitt S.R., Rendell A.P., Roskop L.B., Ruedenberg K. Recent developments in the general atomic and molecular electronic structure system. *J. Chem. Phys.* 2020. **152**: 154102.
72. Marenich A.V., Cramer C.J., Truhlar D.G. Universal solvation model based on solute electron density and on a continuum model of the solvent defined by the bulk dielectric constant and atomic surface tensions. *J. Phys. Chem. B.* 2009. **113**(18): 6378.
73. Stewart J.J.P. *MOPAC2022*. Stewart Computational Chemistry. web: HTTP://OpenMOPAC.net. 2023. (accessed on 30.09.2023, Ver. 22.1).
74. Pettersen E.F., Goddard T.D., Huang C.C., Meng E.C., Couch G.S., Croll T.I., Morris J.H., Ferrin T.E. UCSF ChimeraX: Structure visualization for researchers, educators, and developers. *Protein Sci.* 2021. **30**(1): 70.
75. *Avogadro 2*. https://two.avogadro.cc/. Ver. 1.98.1. 2023.
76. Pedretti A., Mazzolari A., Gervasoni S., Fumagalli L., Vistoli G. The VEGA suite of programs: a versatile platform for cheminformatics and drug design projects. *Bioinformatics.* 2021. **37**(8): 1174.
77. *Jmol: an open–source Java viewer for chemical structures in 3D* (Ver. 16.1.47). http://www.jmol.org/.
78. Gun'ko V.M. Atomic charge distribution functions as a tool to analyze electronic structure of molecular and cluster systems. *Intern. J. Quantum Chem.* 2021. **121**(14): e26665.

*Received 04.01.2024, accepted 03.09.2024*